Soil Dynamics and Earthquake Engineering 164 (2023) 107618

Contents lists available at ScienceDirect

Soil Dynamics and Earthquake Engineering

journal homepage: www.elsevier.com/locate/soildyn

Inspection and repair considerations for downtime assessment of seismically isolated buildings

Shoma Kitayama [a,*], Enrique Abel Morales Moncayo [b], Anastasia Athanasiou [c]

[a] School of Civil Engineering, University of Leeds, Leeds, LS2 9JT, United Kingdom
[b] Department of Earth Sciences and Construction, Armed Forces University (ESPE), Sangolqui, 171103, Ecuador
[c] Department of Building, Civil and Environmental Engineering, Montreal, QC, H3G 2W1, Canada

ARTICLE INFO

Keywords:
Downtime
Seismic isolation
ASCE/SEI 7
Inspection
Repair
Performance evaluation
Life-cycle analysis

ABSTRACT

This paper investigates the seismic downtime of seismically isolated buildings with steel moment or braced frames designed by the procedures of ASCE/SEI 7–16. The seismic isolation systems considered in this study are comprised of triple or double friction pendulum isolation bearings with and without moat walls. The seismic downtime is calculated from the damage to structural components and non-structural components, demolition and collapse of buildings. The downtime components (repair and inspection) are defined, and mathematical expressions are provided for the computation of downtime fragility curves, expected annual downtime, and economic losses due to the expected annual downtime. The procedure is then implemented using the results of nonlinear response history analysis from previous studies by the first author. The study demonstrates that the expected annual downtime of seismically isolated buildings is less than that of the comparable non-isolated buildings regardless of the seismic isolation systems used. Among the cases of seismically isolated buildings studied in this paper, it is found that the most effective structural system to mitigate long downtime is the seismically isolated building with seismic isolators with enhanced sizes and with braced frames that are designed to be minimally compliant with the seismic design requirements of ASCE/SEI 7–16.

1. Introduction

The downtime of buildings after the earthquake causes business discontinuity in office and industrial buildings and evacuation of people for residential buildings (see Fig. 1). For building owners to avoid financial risks, buildings that maintain post-earthquake functionality are economically attractive [1]. In addition, some buildings, such as hospital buildings, play a critical role in treating injuries during earthquake disaster emergency responses [2]. For the buildings that play an essential role in emergency response, continued functionality is expected even under strong earthquake events. However, many buildings, including hospital buildings, experienced loss of functionality and long downtime after recent earthquake events (see Fig. 1). Thus, it is important to consider downtime as a measure of seismic performance of buildings.

The economic loss due to downtime is called the indirect loss [3], whereas the economic loss due to repair, demolition and rebuilding of a damaged building is called direct loss [3,4]. Structural engineers have recognized the indirect loss due to downtime as an important indicator of the seismic performance of buildings, since it is related to the recovery of buildings in the aftermath of a destructive seismic event; moreover it is a quantifiable metric that is also intuitively understood by stakeholders [5]. [6] reported that most business owners can afford to close their businesses for a week for clean up, but not a month or more. By recognizing the importance of downtime after a strong earthquake, structural engineering associations and construction industries proposed rating systems for the quantification of seismic performance of buildings, based on the duration of downtime. For example, the Structural Engineers Association of Northern California [7] introduced a rating system (Earthquake Performance Rating System, EPRS) that considered downtime as one of the dimensions to determine earthquake performance rating of buildings with minimum of 1 to a maximum of 5 stars. The U.S. Resiliency Council (USRC) was formed to implement the SEAONC building rating system. The SEAONC granted the USRC permission to use the work and property described in the SEAONC's EPRS [8]. A structural engineering company, ARUP, proposed three levels of rating for the seismic performance of buildings under the Design Level Earthquake (= 475 years return period ground shaking),

* Corresponding author.
E-mail addresses: s.kitayama@leeds.ac.uk (S. Kitayama), eamorales5@espe.edu.ec (E.A. Morales Moncayo), anaj.athanasiou@gmail.com (A. Athanasiou).

https://doi.org/10.1016/j.soildyn.2022.107618
Received 16 August 2022; Received in revised form 13 October 2022; Accepted 21 October 2022
Available online 1 November 2022
0267-7261/© 2022 The Authors. Published by Elsevier Ltd. This is an open access article under the CC BY license (http://creativecommons.org/licenses/by/4.0/).

those are: Platinum (functional recovery is achieved within 72 h after earthquake), Gold (functional recovery is achieved within 1 month after an earthquake) and Silver (functional recovery is achieved within 6 months after an earthquake) [5,9].

Comerio [10] classified downtime components into rational and irrational components. The rational component of downtime is the time for repairing damaged buildings and refurbishing spaces for use, while the irrational component is the time for financing, relocation of building functions, human resource activities, and the time associated to economic and regulatory uncertainties. Some of these irrational components affect the downtime by delaying the repair initiation. Such initial delay may take longer time than the repair time itself (i.e., rational component), leading to a significant increase of the time required to achieve any recovery state [11]. The initial delay before construction begins is called mobilization time [12] or impeding factors [5,9]. Mobilization time includes the times for damage assessment, consultation with professional engineers and contractor bidding process. For example, if there is an agreement on the damage extent (minor or major), the decision on reopening the building or on keeping it closed is made sooner [10]. If, however, the residual strength of the structural system or operational capacity of the nonstructural systems are not known, the building may have to remain closed until the completion of further review and analysis [10]. To quantify the mobilization time, Mitrani-Reiser et al. [13] introduced the "Virtual Inspector", a framework using the damage states of structural elements of buildings to determine the structural conditions as red, yellow or green placard (based on ATC-20 guidelines' post-earthquake safety evaluation, 1989 [14]; and its updates) and then to compute mobilization time. Note that there is a possibility that utility disruption causes a delay in the initiation of repair actions [15,16]. In such case, the maximum of these two delay times (i.e., utility disruption and mobilization time or impeding factor) is used and then summed with the repair time to compute total downtime [15].

Regarding the framework of seismic performance assessment of buildings that considered downtime, Porter et al. [17] developed the Assembly-Based Vulnerability (ABV) methodology that estimated the repair time of a building using detailed building models and fragility data of structural and non-structural components that were associated with repair time. Mitrani-Reiser [12] developed a probabilistic method to compute downtime. The downtime considered in this study included repair time and time due to change-of-trade delay based on [17,18]; and mobilization time. FEMA P-58 [19] adopted the methodology of [12] to

Fig. 1. Photographs of buildings in the city of Bahía de Caráquez, Manabí province, Ecuador, that experienced long seismic downtime after the 2016 Ecuador earthquake: (a) and (b) a residential building with visible structural damage that led to the loss of functionality and issue of inspection tag (photos were taken by the first author in September 2019); (c), (d) and (e) exterior and interior views of the Miguel H. Alcívar hospital building that lost functionality (photos were taken by the second author in May 2016).

estimate the repair time (rational component), but it did not consider the irrational components of downtime (i.e., mobilization time or impeding factor) described above. ARUP developed a seismic performance rating system for buildings (REDi™ [5,9]). REDi™ introduced a computational method for downtime that went beyond the repair time estimates of FEMA P-58 [19] and that accounted for several irrational components of downtime – utility disruption and delays due to inspection, financing, engineering and contractor mobilization and permitting – however, the accuracy of the predictions of each of the irrational components of downtime remained uncertain due to the lack of validation studies [20]. Note that a recent study by Hutt et al. [21] implemented the downtime computation methods of FEMA P58 [19] and REDi™ [5,9] and estimated the downtime of non-isolated high-rise buildings in San Francisco, California, USA.

Several recent studies have used downtime as one of the measures to assess the seismic performance of seismically isolated buildings. Most of these studies started by performing nonlinear response history analysis of buildings, and then used the results of the nonlinear response history analysis as input into the Performance Assessment Calculation Tool [22] to compute repair time. Terzic et al. [23] evaluated the repair time of seismically isolated buildings with Intermediate Moment Resisting Frames (IMRF), isolated at the base with lead-plug rubber isolation bearings or triple friction pendulum isolation bearings, and comparable non-isolated buildings with Special Moment Resisting frames (SMF), designed as per ASCE/SEI 7–05 [24]. The study considered three different seismic intensity levels (50% in 50-year, 10% in 50-year and 2% in 50-year hazard levels) and demonstrated that, regardless of the seismic hazard level and regardless of the seismic isolation systems considered, the increase of the strength of superstructure reduces the computed repair time. Moretti et al. [25] and Cimellaro et al. [26] investigated the seismic performance of 3-story non-isolated steel buildings with SMF and 3-story seismically isolated buildings with IMRFs, designed according to ASCE/SEI 7–10 (2010) [27]. Their studies demonstrated that the repair times of non-isolated buildings were three to six times longer than the repair times of the isolated buildings depending on the occupancy types and the intensity of the seismic event. Moreover, the studies showed that under the earthquake motion with 10% probability of exceedance in 50 years level, the repair times for non-isolated buildings used as healthcare facilities were 78–207 days (depending on the repair strategies), whereas those for comparable isolated buildings were 19–45 days. Cutfield et al. [28] studied the life cycle cost of seismically isolated 3-story steel buildings with Ordinary Concentrically Braced Frames (OCBFs) and non-isolated buildings with steel Special Concentrically Braced Frames (SCBFs) that were designed based on the minimum requirements in ASCE/SEI 7–05 [24]. The computed downtime duration was converted to dollar loss. The study found that the Expected Annual Losses (EALs) accounting for both repair cost and cost from mobilization time were 7–10 times higher than the EALs accounting for only repair cost for both isolated and non-isolated buildings. Mayes et al. [11] studied the seismic performance of buildings with various seismic protective systems, including seismically isolated buildings with braced frames (designed based on the 1997 Uniform Building Code [29]), buildings with moment frames and viscous dampers, Buckling Restrained Braced Frames, SMFs and reinforced concrete shear walls. The study presented the results from PACT [22] that compared the repair times between different structural systems for the earthquake events of the 475-year return period. Among all the compared systems, only the seismically isolated building could achieve a median repair time that was less than a month. Molina Hutt et al. [15] studied the seismic performance of high-rise buildings with SMF that were designed based on the procedures of ASCE/SEI 7–10 standard [27]. The study investigated different performance enhancement options, such as strengthening the structure by introducing an elastic spine throughout the building core, using seismic isolation at the base of the building, seismically strengthening nonstructural components or combinations of these options. The downtime was computed using the methods in FEMA P58 [22] and REDi™ [5,9] that consider both the rational and irrational components of downtime. The study demonstrated that the downtime for both re-occupancy and functional recovery was reduced to about a day when both the seismic isolation and seismically strengthened non-structural components were used. Dong and Frangopol [30] studied the seismic performance of 3-story seismically isolated steel buildings with IMRFs and non-isolated buildings with SMF (both buildings were designed by ASCE/SEI 7–05 [24]) under the two seismic ground motions that were scaled to the design earthquake level, in terms of repair loss, fatality loss, CO_2 emissions, and repair time. The repair time was calculated based on [17]. The study considered two different repair schemes: slow-track and fast-track. The slow-track is a repair scheme where components are repaired serially (i.e., each floor is repaired one-by-one); and the fast-track is a repair scheme where components are repaired in parallel (i.e., all floors are repaired simultaneously). The results of downtime from different seismic ground motions and from different repair schemes differed significantly. It was shown that when seismic isolation was used, the repair time could be reduced to 1–2 months (if fast-track is used), whereas the non-isolated buildings might experience about two years of repair time (if slow-track is used) for the design earthquake shakings.

This paper investigates the seismic performance of seismically isolated and comparable non-isolated 6-story buildings with SCBFs and SMFs in terms of downtime. The buildings, shown in Fig. 2, were designed by the procedures of ASCE/SEI 7–16 [31] and further details can be found in Kitayama and Constantinou [32–35]. The total seismic weight of the building when seismically isolated is 53,670 kN. When non-isolated the weight is 45,285 kN. The building is assumed to be located on soil class D in San Francisco, CA (Latitude 37.783°, Longitude −122.392°) with Risk-Targeted Maximum Considered Earthquake (MCE_R) spectral acceleration values of $S_{MS} = 1.5g$ and $S_{M1} = 0.9g$. The results of nonlinear response history analysis obtained by Refs. [32–35] are used in this study as input to compute downtime according to the procedures described in the present study. The key findings from the studies in Refs. [32–35] were that the seismically isolated buildings designed by the minimum requirements of ASCE/SEI 7–16 [31] may have unacceptable probabilities of collapse in the MCE_R, whereas comparable non-isolated structures, also designed by the minimum criteria of ASCE/SEI 7–16 [31], had acceptable probabilities of collapse. In terms of other seismic demands (i.e., peak story drift ratio, peak residual story drift ratio, peak floor acceleration), it was demonstrated that the annual frequencies of exceedance of these seismic demands of seismically isolated buildings were smaller than those of comparable non-isolated buildings for wide range of seismic demands. The details of designs, models and procedures for nonlinear response history analysis of seismically isolated and non-isolated buildings can be found in Refs. [32,33]. The results of nonlinear response history analysis used in this study (originally reported in Refs. [32–35] include peak story drift ratio, peak residual story drift ratio, peak floor acceleration and collapse capacities. This paper first outlines the methodology to compute downtime. The procedure used in this study is based on [12,13] but extends such studies by explicitly considering the influence of residual story drift on the computed downtime based on [36]. This paper then describes the component fragility curves that are specific to the considered buildings and that are used within the methodology. Then, the seismic downtime assessment is performed, and the results of the assessment are presented and discussed. Finally, the conclusion section summarizes the study presented and findings made in this paper.

2. Methodology for downtime estimation

The downtime assessment methodology presented in this paper considers the time for repair effort (rational component) needed to return damaged building elements to their undamaged state, as well as the time for safety tagging that is one of the mobilization times (irrational component). Other irrational components of downtime, such as utility

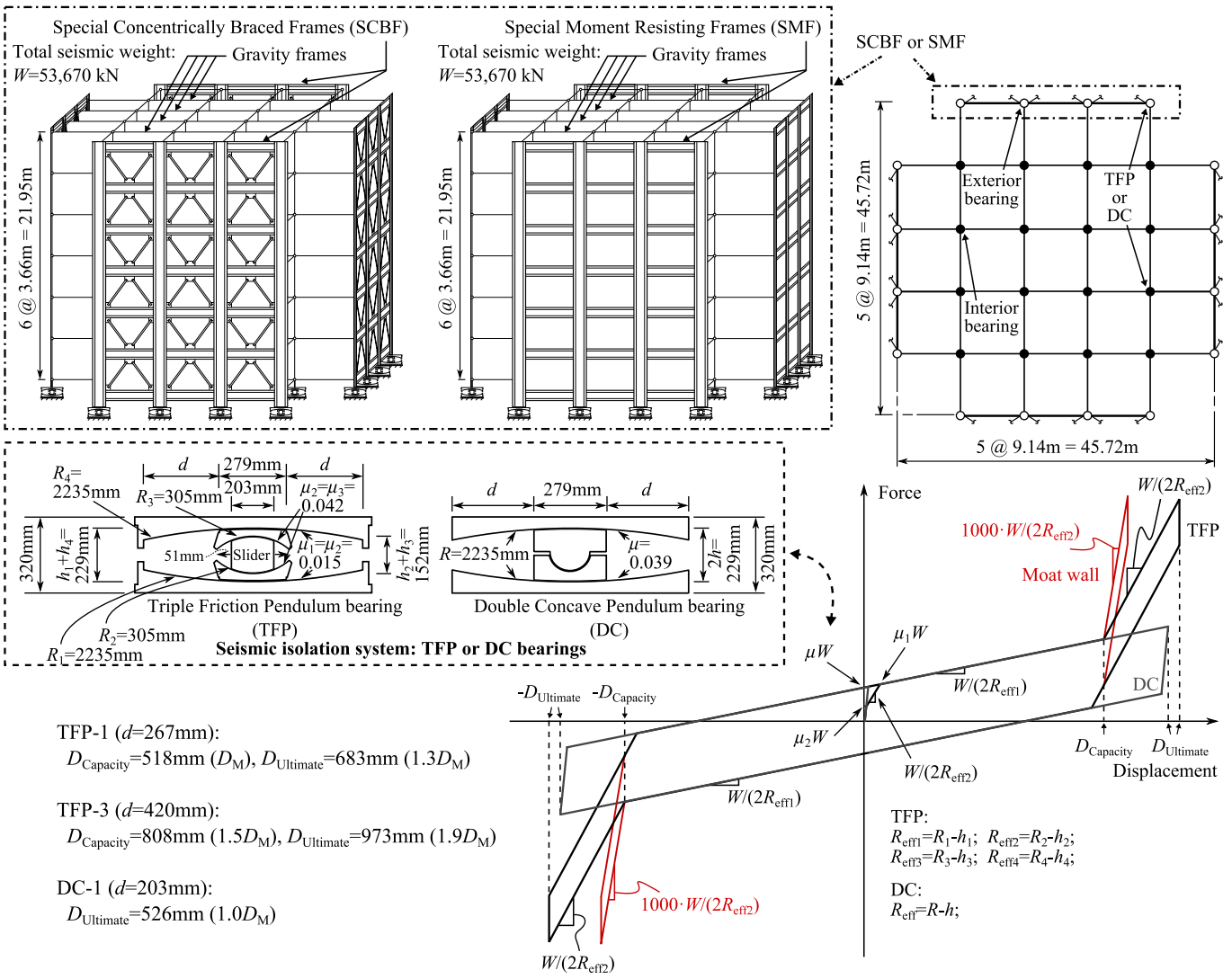

Fig. 2. Case study building geometry, isolators' properties and associated hysteretic model, from Ref. [32].

disruptions, may also contribute to the total downtime [15,16]; however, such components were not considered herein due to the insufficient information available for their estimation. The assessment procedure presented herein was programmed in MATLAB (version 9.10.0.1649659, R2021a, Update 1; The MathWorks, Inc). Source codes and associated documents are available on an online repository [37].

2.1. Overview

This study computes downtime based on the methodology proposed by Mitrani-Reiser [12]. To include the effect of demolition of buildings (and subsequent reconstruction of buildings) due to large residual story drift on the downtime computation, the framework developed by Ramirez and Miranda [36] is incorporated in the methodology. The data from the results of nonlinear response history analysis in Kitayama and Constantinou [32,33] in terms of peak floor acceleration, peak and residual story drift ratio (Engineering Demand Parameters or EDP) and probability of collapse, are used in this study. The seismic response analysis in Refs. [32,33] was conducted by using the Conditional Spectra procedure described in Refs. [38,39] to select and scale ground motion records so that the ground motion records for the seismic response analysis are representative of a various intensity of earthquake events (i.e., frequent to rare seismic events). More information on the ground motion selection, scaling, nonlinear response history analysis and models and designs for the buildings studied in this paper can be found in Refs. [32–35]. As an example, ground motions that were selected and scaled for the seismic response analysis of the considered seismically isolated buildings (effective period of 3.66 s), target Conditional Spectra (CS; [38,39]) with target variations of ± 2σ, and Conditional Mean Spectra (CMS; [40]) for 10 different return periods are shown in Fig. 3.

2.2. Formulas

2.2.1. Downtime computation

Firstly, the mean value of the repair time for an operational unit m, $E[R^*_U(m)]$, under seismic event with an intensity IM = im that does not cause the collapse of the structure (NC), is calculated from Eq. (1) based on [12]. The repair time R^*_U is measured in calendar days, starting from the commencement date of the repair works.

$$E\left[R^*_U(m)\middle|\mathrm{NC}, im\right] = \frac{\sum_{i=1}^{na(m)}\left\{Nu_i(m)\bullet\sum_{j=1}^{ndsi}E\left[R_i\middle|DS_{ij}\right]\bullet P\left[DS_{ij}\middle|NC, im\right]\right\}}{wh\bullet wr\bullet cn} + N_T(m)\bullet E[R_{COT}] \quad (1)$$

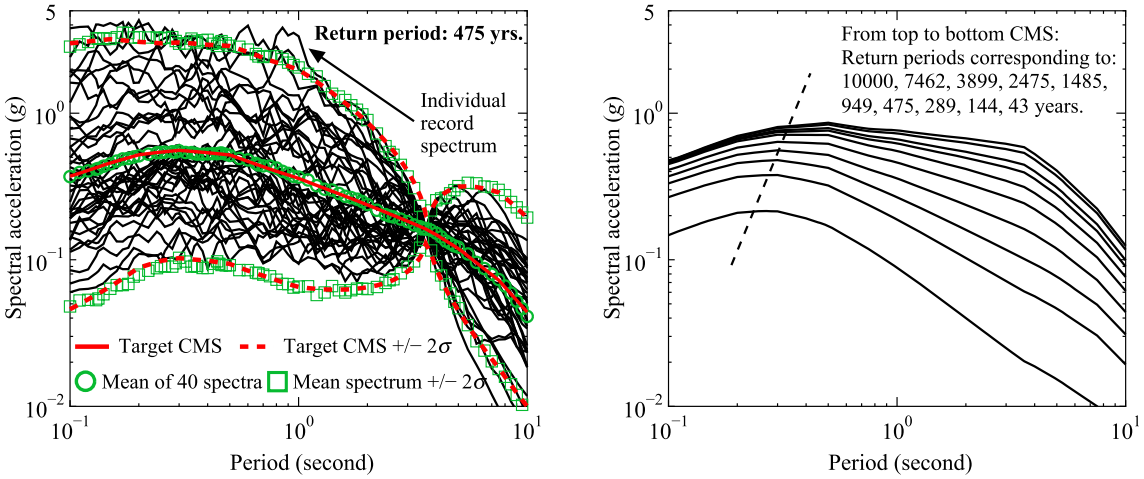

Fig. 3. Example acceleration response spectra of selected ground motions with CS as target spectra for response history analysis of seismically isolated buildings with lower bound isolator properties (T = 3.66 s).

where $na(m)$ is the number of assembly groups in the operational unit m; $Nu_i(m)$ is the number of units in damageable assembly group i located in operational unit m; DS_{ij} is damage state j for a given building for assembly group i; nds_i is the number of damage states of the assembly group i; R_i is the repair time for one unit of the assembly group i (see Table 1); $N_T(m)$ is the number of changes-of-trade in operational unit m; and R_{COT} is the change-of-trade delay (assumed to be the same for each trade). Note that an assembly group is defined as the set of damageable assemblies of the same type that are sensitive to the same EDP; and an operational unit is defined as each story [12]. Also, note that Eq. (1) is based on Eqs. (6-1) to (6-5) in Ref. [12] but was modified according to Ref. [30] to include explicitly the terms *wh*, *wr* and *cn*, where *wh* is the workday hours, *wr* is a workday ratio, and *cn* is the number of crews. Based on [12]; wh=(8 + 7)/24 = 0.625 (i.e., in each day of 24 h, day-time crews work for 8 h and night-time crews work for 7 h). Also based on [30], wr = 5/7 = 0.714 (i.e., Monday-Friday: Workdays; Saturday-Sunday: Holidays) and cn = 15 (i.e., 15 crews per floor). Mitrani-Reiser [12] and Porter et al. [17] estimated that the values for R_{COT} is 2 days and 14 days under fast-track and slow-track repair schemes, respectively. Beck et al. [18]. defined that the change-of-trade delay as the delay between the repairs of two damaged assemblies. Additionally, based on [12], there is no change-of-trade between the repairs of different structural components (see "Category" in Table 1), whereas there is change-of-trade between the repairs of different assemblies within non-structural components. Thus, in this study, the value of $N_T(m)$ is determined by checking damage states of structural and non-structural components from EDPs to know how many assembly groups are damaged at the operational unit m (i.e., counting the number of assembly groups that exceed arbitrary small probability of initial damage state, DS_{i1}; 5% is assumed in this study). Thus, in this study, the values for $N_T(m)$ is determined such that, for each operational unit (i.e., each story), $0 \le N_T(m) \le 6$ (there are six non-structural components, including drift and acceleration sensitive non-structural components, see Table 1); $P[DM_{ij}|NC, im]$ is the probability of exceeding the damage state j for a given assembly group i, conditioned on the structure not collapsing (NC), which is obtained as follow:

$$P\left[DS_{ij}|NC, im\right] = \int_0^\infty P\left[DS_{ij}|EDP\right] \bullet f\left[EDP|IM\right] \bullet d\mathrm{EDP} \tag{2}$$

where $f[EDP|IM]$ is the probability density function of the EDP given an IM = im; $P[DS_{ij}|EDP]$ is the probability of the EDP of interest (eg. peak floor acceleration) associated with the ith assembly group exceeding the jth damage state given an EDP = edp. Note that $f[EDP|IM]$ is assumed to follow a lognormal distribution defined by the median and logarithmic standard deviation. The $P[DS_{ij}|EDP]$ is calculated as follows [41]:

$$P\left[DS_{ij}|EDP\right] = \begin{cases} 1 - F_{\mathrm{DS}_{i1}}(\mathrm{EDP}) \bullet F_{\mathrm{DS}_{i1}}(\mathrm{GP}) & (j = 0) \\ F_{\mathrm{DS}_{ij}}(\mathrm{EDP}) \bullet F_{\mathrm{DS}_{ij}}(\mathrm{GP}) - F_{\mathrm{DS}_{i(j+1)}}(\mathrm{EDP}) \bullet F_{\mathrm{DS}_{i(j+1)}}(\mathrm{GP}) & (1 \le j \le n) \\ F_{\mathrm{DS}_{ij}}(\mathrm{EDP}) \bullet F_{\mathrm{DS}_{ij}}(\mathrm{GP}) & (j = n) \end{cases} \tag{3}$$

where $F_{\mathrm{DS}_{ij}}(\mathrm{EDP})$ is the fragility curve (=lognormal cumulative distribution function, exceedance probability) for the ith component being in the jth damage state conditioned on an EDP = edp; $F_{\mathrm{DS}_{ij}}(\mathrm{GP})$ is the cumulative distribution function for the ith component being in the jth damage state conditioned on a geometric parameter GP = gp. Note that in this study, the dependence of the geometry on the component fragility curves is only considered for braces in SCBF, hence $F_{\mathrm{DS}_{ij}}(\mathrm{GP}) = 1$ for all SMF components at the considered damage states, and $F_{\mathrm{DS}_{ij}}(\mathrm{GP}) \neq 1$ for SCBF braces at the considered damage states (the details of $F_{\mathrm{DS}_{ij}}(\mathrm{GP})$ are discussed in the next section and Table 2). $F_{\mathrm{DS}_{ij}}(\mathrm{GP})$ is essentially a factor to modify $F_{\mathrm{DS}_{ij}}(\mathrm{EDP})$ to consider the influence of steel brace global and local slenderness on the steel brace damage states. $F_{\mathrm{DS}_{ij}}(\mathrm{GP})$ depends on the database developed by Lignos and Karamanci [42].

The mean total repair time (a rational component of downtime)

Table 1
Median values and dispersion factors of component fragility curves $F_{DS_{ij}}(EDP)$ and repair time parameters for buildings with SCBF and SMF.

Category	Damageable assembly group (=i)	Damage State (DS)	Unit	Fragility parameters			Repair time	Assembly quantity (total)
				EDP	μ_{EDP}	β_{lnEDP}	$E[R_i\|DM_{ij}]$ (days/person)	
Structural components	Column base (W < 223 kg/m)	DS_{i1}	EA	SDR	0.04	0.40	18.7*1	16
		DS_{i2}			0.07	0.40	26.5*1	
		DS_{i3}			0.10	0.40	31.5*1	
	Column base (223 kg/m < W ≤ 446 kg/m)	DS_{i1}	EA	SDR	0.04	0.40	14.8*1	
		DS_{i2}			0.07	0.40	21.6*1	
		DS_{i3}			0.10	0.40	27.0*1	
	Column base (446 kg/m < W)	DS_{i1}	EA	SDR	0.04	0.40	14.1*1	
		DS_{i2}			0.07	0.40	21.6*1	
		DS_{i3}			0.10	0.40	27.7*1	
	Column splices (W < 223 kg/m)	DS_{i1}	EA	SDR	0.04	0.40	9.17*1	64
		DS_{i2}			0.07	0.40	10.9*1	
		DS_{i3}			0.10	0.40	10.9*4	
	Column splices (223 kg/m < W ≤ 446 kg/m)	DS_{i1}	EA	SDR	0.04	0.40	7.53*1	
		DS_{i2}			0.07	0.40	9.57*1	
		DS_{i3}			0.10	0.40	9.57*4	
	Column splices (446 kg/m < W)	DS_{i1}	EA	SDR	0.04	0.40	7.57*1	
		DS_{i2}			0.07	0.40	9.80*1	
		DS_{i3}			0.10	0.40	9.80*4	
	Column (≤W27)	DS_{i1}	EA	SDR	0.03	0.30	10.2*1	192
		DS_{i2}			0.04	0.30	17.2*1	
		DS_{i3}			0.05	0.30	17.2*1	
	Column (≥W27)	DS_{i1}	EA	SDR	0.03	0.30	10.8*1	
		DS_{i2}			0.04	0.30	19.1*1	
		DS_{i3}			0.05	0.30	19.1*1	
	Round HSS (Weight<60 kg/m) (SCBF only)	DS_{i1}	EA	SDR	0.0041	0.51	19.8*1	144
		DS_{i2}			0.0096	0.45	22.9*1	
		DS_{i3}			0.0275	0.51	24.1*1	
	Round HSS (61 kg/m < Weight<147 kg/m) (SCBF only)	DS_{i1}	EA	SDR	0.0041	0.51	19.8*1	
		DS_{i2}			0.0096	0.45	29.2*1	
		DS_{i3}			0.0275	0.51	31.7*1	
	Moment connection (one-sided ≤ W27) (SMF only)	DS_{i1}	EA	SDR	0.03	0.30	10.2*1	48
		DS_{i2}			0.04	0.30	17.2*1	
		DS_{i3}			0.05	0.30	17.2*1	
	Moment connection (one-sided ≥ W27) (SMF only)	DS_{i1}	EA	SDR	0.03	0.30	10.8*1	
		DS_{i2}			0.04	0.30	19.1*1	
		DS_{i3}			0.05	0.30	19.1*1	
	Moment connection (two-sided ≤ W27) (SMF only)	DS_{i1}	EA	SDR	0.03	0.30	20.6*1	48
		DS_{i2}			0.04	0.30	30.8*1	
		DS_{i3}			0.05	0.30	30.8*1	
	Moment connection (two-sided ≥ W27) (SMF only)	DS_{i1}	EA	SDR	0.03	0.30	20.6*1	
		DS_{i2}			0.04	0.30	34.4*1	
		DS_{i3}			0.05	0.30	34.4*1	
	Shear tab connections	DS_{i1}	EA	SDR	0.04	0.40	11.8*1	624 (SCBF)
		DS_{i2}			0.08	0.40	12.0*1	480 (SMF)
		DS_{i3}			0.11	0.40	11.9*1	
	Corrugated slab*2*3	DS_{i1}	m^2	SDR	0.00375	0.13	0.096*2*3	10,535
		DS_{i2}			0.01	0.22	0.500*2*3	
		DS_{i3}			0.05	0.35	5.417*2*3	
Non-structural components (Drift-sensitive)	Drywall partition	DS_{i1}	$6m^2$	SDR	0.0039	0.17	0.042*2	1,756
		DS_{i2}			0.0085	0.23	0.167*2	
	Drywall finish	DS_{i1}	$6m^2$	SDR	0.0039	0.17	0.042*2	1,756
		DS_{i2}			0.0085	0.23	0.292*2	
	Exterior glazing	DS_{i1}	Pane	SDR	0.04	0.36	0.479*2	1,427
		DS_{i2}			0.046	0.33	0.479*2	
Non-structural components (Acceleration-sensitive)	Suspended Ceiling, SDC D,E (I_p = 1.0), Area (A): A > $232m^2$, Vert & Lat support*1	DS_{i1}	$232m^2$	PFA (g)	1.09*1	0.30*1	3.00*1	45
		DS_{i2}			1.69*1	0.30*1	24.3*1	
		DS_{i3}			1.91*1	0.30*1	49.8*1	
	Braced automatic sprinklers*5	DS_{i1}	3.66 m	PFA (g)	32*5	1.40*5	0.625*2	786
	Elevator	DS_{i1}	EA	PGA (g)	0.50	0.28	2.5*2	2

EA = Each component.
SDR=Story drift ratio.
PFA=Peak floor acceleration; PGA=Peak ground acceleration.
$E[R_i|DM_{i0}] = 0$.
Repair time for corrugated slab and drywall finish is not considered because of the unavailability of repair time information.
*1: From fragility specification document (version 3.1.2) in Ref. [19].
*2: From Chapters 2 and 6 in Ref. [12].
*3: Assumed to be the same as Column-slab connections in Chapters 2 and 6 in Ref. [12].
*4: There was no information in Ref. [19]; thus the same values to lower damage states are assumed.
*5: From B.5.1. in Ref. [43].

Note: The section properties of the gravity frames used in loss calculation for columns and beams are determined based on the previous studies (SEAOC, 2014; McVitty and Constantinou, 2015). The following gravity columns were considered: W12 × 96, W12 × 58 and W12 × 35 for 1st and 2nd stories, 3rd and 4th stories and 5th and 6th stories, respectively. Also, the following gravity beams were considered: W33x118 for the 1st floor (isolated buildings only) and W21x44 for other floors (both isolated and non-isolated buildings).

Table 2
Median values and dispersion factors of component fragility curves $F_{DS_{ij}}(GP)$ for braces in SCBF (data from [42].

Assembly description		Fragility parameters	
	Damage state	$\mu_{KL/r}$	$\beta_{\ln KL/r}$
Round HSS brace	DS_{i1}	63.6	0.46
	DS_{i2}	66.1	0.45
	DS_{i3}	68.9	0.40

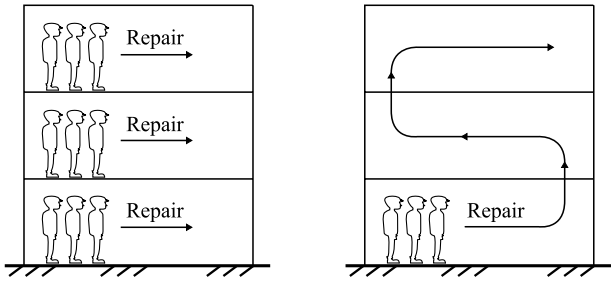

Parallel repair strategies (fast-track) Serial repair strategies (slow-track)

Fig. 4. Fast- and slow-track repair strategies.

conditioned on the structure not collapsing, measured in calendar days from the date on which repair work is begun, and on a seismic intensity IM = *im* is calculated as follows [12]:

$$E[R_T|\mathrm{NC},im]=\begin{cases}\max\left\{E\left[R_U^*(m)\middle|NC,im\right],m=1,\ldots,nou\right\} & (\text{Fast}-\text{track repair scheme})\\ \sum_{m=1}^{nou}E\left[R_U^*(m)\middle|NC,im\right] & (\text{Slow}-\text{track repair scheme})\end{cases} \quad (4)$$

where *nou* is the number of operational units (=number of the story). Note that FEMA P-58 [19] defines that in parallel repair strategies (i.e., fast-track) work occurs on all stories simultaneously; and in serial repair strategies (i.e., slow-track) work occurs sequentially between stories. Fig. 4 illustrates those two repair strategies.

For the mobilization time (irrational component of downtime) $E[R_{T0}|NC,im]$ to be considered as part of downtime, the downtime is calculated as the sum of repair time and mobilization time as follows:

$$E[R_{T+T0}|\mathrm{NC},im]=E[R_T|\mathrm{NC},im]+E[R_{T0}|\mathrm{NC},im] \quad (5)$$

The mobilization time, $E[R_{T0}|NC,im]$, is determined based on post-earthquake inspection results. After a strong earthquake event, teams of volunteers and industry professionals are assembled and tasked with inspecting and "tagging" each building (Applied Technology Council, 1995 [44]; see also Fig. 1 (b)). Post-earthquake inspection and tagging are necessary to identify safe and unsafe buildings, and to avoid death and injuries resulting from aftershocks [45,46]. Buildings that are safe for re-occupancy are assigned a green tag, whereas those that are unsafe for re-occupancy are assigned a red tag. In cases where the extent to which the potential danger of re-occupancy is less obvious and further assessment is required, the buildings are assigned a yellow tag [47]. This study assumes that the yellow tag will be eventually replaced with either a green tag or a red tag since the additional assessment when a yellow tag is assigned often leads to the tag re-assignment as green or red [47]. Thus, the mobilization time is computed based on the theorem of total probability, conditioned on the structure not collapsing (NC) and conditioned on the building safety-tagging results as follow (note, G: Green, R: Red):

$$E[R_{T0}|NC,im]=E[R_{T0}|\mathrm{TAG}=G]\bullet P[\mathrm{TAG}=G|\mathrm{NC},im]+E[R_{T0}|\mathrm{TAG}=R]\bullet P[\mathrm{TAG}=R|\mathrm{NC},im] \quad (6)$$

where $E[R_{T0}|\mathrm{TAG}=G]$ and $E[R_{T0}|\mathrm{TAG}=R]$ are the mean mobilization times when tagged green and red, respectively; $P[\mathrm{TAG}=G|\mathrm{NC},im]$ and $P[\mathrm{TAG}=R|\mathrm{NC},im]$ are the probability of receiving green and red tags, respectively. Mitrani-Reiser [12] estimated that $E[R_{T0}|\mathrm{TAG}=G]$ is 10 days and $E[R_{T0}|\mathrm{TAG}=R]$ is 6 months, which are used in this paper. Eqs. (7) and (8) evaluate $P[\mathrm{TAG}=G|\mathrm{NC},im]$ and $P[\mathrm{TAG}=R|\mathrm{NC},im]$ following the work of [13] (note, Y: Yellow):

$$P[\mathrm{TAG}=G|\mathrm{NC},im]=P[\mathrm{TAG}=G|im,\mathrm{RE}]+P[\mathrm{TAG}=G|im,\mathrm{DE}]\bullet P[\mathrm{TAG}=Y|im,\mathrm{RE}] \quad (7)$$

$$P[\mathrm{TAG}=R|\mathrm{NC},im]=P[\mathrm{TAG}=R|im,\mathrm{RE}]+P[\mathrm{TAG}=R|im,\mathrm{DE}]\bullet P[\mathrm{TAG}=Y|im,\mathrm{RE}] \quad (8)$$

where $P[\mathrm{TAG}=G|im,\mathrm{RE}]$, $P[\mathrm{TAG}=Y|im,\mathrm{RE}]$ and $P[\mathrm{TAG}=R|im,\mathrm{RE}]$ are the probabilities of building being green-tagged (G), yellow-tagged (Y) and red-tagged (R), respectively, after rapid evaluation; and $P[\mathrm{TAG}=G|im,\mathrm{DE}]$ and $P[\mathrm{TAG}=R|im,\mathrm{DE}]$ are the probabilities of a building being green-tagged and red-tagged, respectively, after detailed evaluation. The sequence of tag-assignment considered in this study is illustrated in Fig. 5. Note that the sequence of tag-assignment in Fig. 5 is based on the event tree model for building safety evaluation reported in Ref. [13]; which was developed based on [14,44]. Also note that the illustration in Fig. 5 is a schematic. In actual inspection, the structural members may be hidden by non-structural components, such as ceiling, external cladding or internal walls. When the structural elements are not exposed, inspectors may remove the non-structural elements to check the damage status of the structural elements. The relationship between the damage state information and different tagging assignment is described in the following paragraph (and also in Fig. 6).

$P[\mathrm{TAG}=G|im,\mathrm{RE}]$, $P[\mathrm{TAG}=Y|im,\mathrm{RE}]$, $P[\mathrm{TAG}=R|im,\mathrm{RE}]$, $P[\mathrm{TAG}=G|im,\mathrm{DE}]$, and $P[\mathrm{TAG}=R|im,\mathrm{DE}]$ in Eqs. (7) and (8) are expressed as follows [13]:

$$P[\mathrm{TAG}=G|im,\mathrm{RE}]=P(\text{Light external structural damage}|im,\mathrm{NC}) \quad (9)$$

$$P[\mathrm{TAG}=Y|im,\mathrm{RE}]=P(\text{Moderate external structural damage}|im,\mathrm{NC}) \quad (10)$$

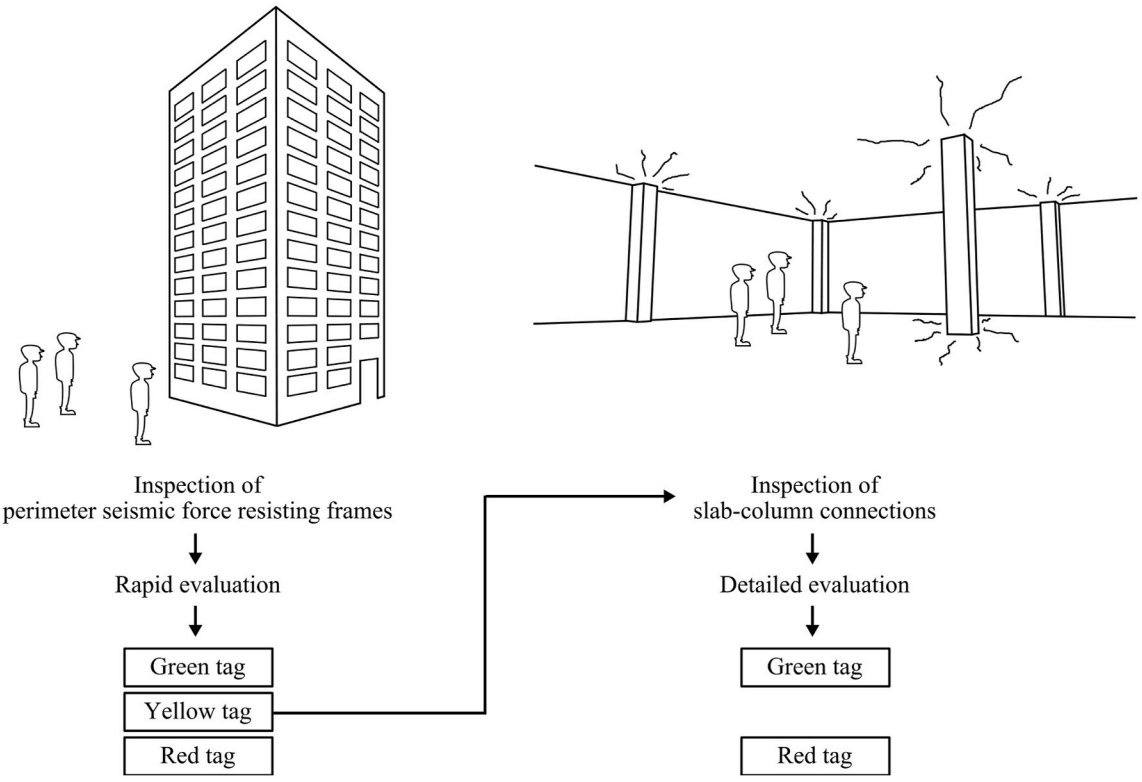

Fig. 5. Safety tagging procedure for perimeter frame buildings.

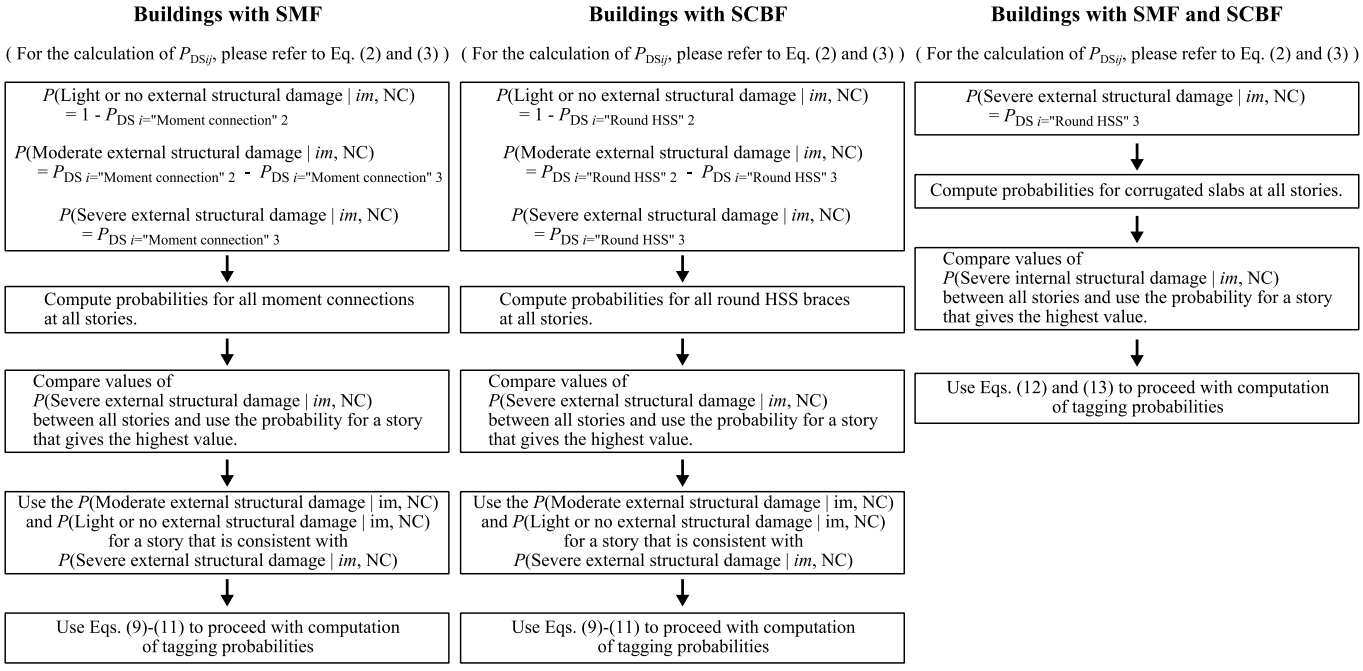

Fig. 6. Workflows relating the damage state information to tagging probability computation, for buildings with SMF and SCBF.

$$P[\mathrm{TAG}=\mathrm{R}|im,\mathrm{RE}]=P(\text{Severe external structural damage}|im,\mathrm{NC}) \quad (11)$$

$$P[\mathrm{TAG}=G|im,\mathrm{DE}]=P(\text{Nonseverer internal structural damage}|im,\mathrm{NC})=1-P[\mathrm{TAG}=\mathrm{R}|im,\mathrm{DE}] \quad (12)$$

$$P[\mathrm{TAG}=\mathrm{R}|im,\mathrm{DE}]=P(\text{Severe internal structural damage}|im,\mathrm{NC}) \quad (13)$$

Based on [12,13], for the perimeter frame designs considered in this study, P(Severe external structural damage|im, NC) is taken as the maximum probability among all the probabilities evaluated for elements in perimeter seismic force-resisting frames with the severest damage state (in this study, the probabilities are obtained by checking the fragility curves of "Moment connections" for SMFs and "Round HSS" braces for SCBFs – see Table 1); P(Moderate external structural damage| im, NC) is calculated similarly but using the maximum probability of the

corresponding probabilities of the perimeter frames to experience the second damage states; P(Light external structural damage|im, NC) is also calculated similarly but using the maximum probability of the second damage states not occurring; and P(Severe internal structural damage|im, NC) is taken as the maximum probability of the corresponding probabilities of all the two-way slabs suffering punching shear cracking or failure (i.e., Corrugated slab in Table 1 with DS_{i3} = Shear stud fracture). The computation of these probabilities is explained in Fig. 6. As indicated in Fig. 6, the maximum probabilities (or resultant colors of tags) are determined based on the peak story drift ratios from the nonlinear response history analysis.

As with the seismic loss computations in Refs. [4,36,41], the mean total building downtime for a given hazard level is determined by assuming mutually exclusive and collectively exhaustive events of building collapse and non-collapse, and building demolition and non-demolition as follow:

$$\begin{aligned} E[R_T|im] = {} & E[R_{T+T0}|\mathrm{NC}, im] \bullet (1 - P[D|IM, NC]) \bullet (1 - P[C|IM]) \\ & + E[D_T|\mathrm{NC}] \bullet P[D|IM, NC] \bullet (1 - P[C|IM]) \\ & + E[C_T|\mathrm{C}] \bullet P[C|IM] \end{aligned} \tag{14}$$

where $P[C|IM]$ is the collapse probability given IM = im, $E[C_T|\mathrm{C}]$ is the expected downtime of a building that is judged as collapsed; and $E[D_T|\mathrm{NC}]$ is the expected downtime of a building that is demolished (due to large residual story drift). Based on the estimation in Refs. [12,48], the values of $E[C_T|\mathrm{C}]$ and $E[D_T|\mathrm{NC}]$ are determined as 38 months (each). Note that this value may depend on the building in question, for example, a smaller value was used in Ref. [30] (=23.4 months). In this study, due to the lack of information for estimating $E[C_T|\mathrm{C}]$ and $E[D_T|\mathrm{NC}]$, the more conservative estimation (=38 month) is used. Note that this paper is discussing fairly modern structures (designed based on ASCE/SEI 7–16 [31]) that are not prone to the progressive, pancake collapse that was a popular collapse mechanism in the past [49,50]; the "collapse" considered herein is instead closer to the demolition rather than the outright destruction of the building.

In Eq. (14), $P[D|IM, NC]$ is the probability that the building is considered to be demolished given an IM = im; $P[C|IM]$ is collapse probability given an IM = im. The $P[D|IM, NC]$ in Eq. (14) is obtained by the following equation:

$$P[D|IM, NC] = \int_0^\infty P[D|RSDR] \bullet f[RSDR|IM] \bullet d\mathrm{RSDR} \tag{15}$$

where $f[RSDR|IM]$ is the probability density function of the maximum residual story drift ratio (RSDR) along with the height of the building given an IM = im; $P[D|RSDR]$ is the probability of having to demolish the building conditioned on the maximum RSDR along with the height of the building, which is modelled by lognormal distribution with a median $\mu_{D|\mathrm{RSDR}} = 0.015$ radians and a logarithmic standard deviation $\beta_{\ln D|\mathrm{RSDR}} = 0.3$ [36].

The results of calculation from Eq. (14), which are the downtime vulnerability curves, are integrated with seismic hazard curves to obtain expected annual downtime ($EADT$) as:

$$EADT = \int_0^\infty E[R_T|im] \left| \frac{d\lambda_{\mathrm{IM}}}{dIM} \right| dIM \tag{16}$$

where λ_{IM} is the mean annual frequency of exceeding a particular seismic intensity measure (in this study, spectral acceleration at the fundamental period of vibration was used - see Ref. [33] for the information about λ_{IM} and the fundamental period of vibration of each building).

2.2.2. Economic loss computation due to downtime (indirect loss computation)

This subsection goes a step further calculating the economic loss associated with the estimated downtime (i.e., indirect loss). The types of downtime considered for the economic loss computation are: (a) time for tagging, (b) repair times for damaged structural and non-structural components, (c) time for dealing with the demolition of a building, and (d) time for dealing with the collapse of a building. The economic loss due to downtime, conditioned on seismic intensity IM = im, $E[DTL|im]$, is calculated as the sum of the economic losses resulting from the repair times of all floors and from the tagging time [12], as follows:

$$\begin{aligned} E[DTL|im] = {} & E[DTL|\mathrm{NC}, im] \bullet (1 - P[D|IM, NC]) \bullet (1 - P[C|IM]) \\ & + E[DTL|D_T] \bullet E[D_T|\mathrm{NC}] \bullet P[D|IM, NC] \bullet (1 - P[C|IM]) \\ & + E[DTL|C_T] \bullet E[C_T|\mathrm{C}] \bullet P[C|IM] \end{aligned} \tag{17}$$

$$E[DTL|NC, im] = E[DTL|\mathrm{TAG}] \bullet E[R_{T0}|NC, im] + \begin{cases} \max\left\{E[U_U(m)] \bullet E\left[R_U^*(m)\middle|NC, im\right], m = 1, \ldots, nou\right\} & (\mathrm{Fast-track\ repair\ scheme}) \\ \sum_{m=1}^{nou} E[U_U(m)] \bullet E\left[R_U^*(m)\middle|NC, im\right] & (\mathrm{Slow-track\ repair\ scheme}) \end{cases} \tag{18}$$

Note in this study, the average lease rate of \$1.33/ft^2/month is assumed based on [12,30]. $E[U_U(m)]$ is the mean rent per operational unit calculated from the average lease rate with the leasable building area per operational unit (i.e., $E[U_U(m)]$ = \$1.33/ft^2/month × 18,900 ft^2). Note that the single floor area of building is calculated to be 18, 900ft^2/floor (or 1,756 m^2/floor) for all buildings considered in this study (the total floor area of a building is 113,400 ft^2 or 10,535 m^2). $E[DTL|D_T]$, $E[DTL|C_T]$ and $E[DTL|\mathrm{TAG}]$ are dollar losses for given values of downtime (unit: \$/month) for the events of demolition, collapse and tagging process, respectively. These are calculated from the average lease rate with the total leasable building area (i.e., $E[DTL|D_T] = E[DTL|C_T] = E[DTL|\mathrm{TAG}]$ = \$1.33/ft^2/month × 18900ft^2 × 6). Note that $E[R_U^*(m)|\mathrm{NC}, im]$ is from Eq. (1). Also, note that it was assumed here that the whole building is unusable for the period between the earthquake occurrence and the completion of the tagging inspection. The expected annual economic loss due to downtime is calculated from the following equation [12]:

$$EADTL = \int_0^\infty E[DTL|im] \left| \frac{d\lambda_{\mathrm{IM}}}{dIM} \right| dIM \tag{19}$$

3. Component fragility curves

The evaluation of $P[DS_{ij}|EDP]$ in Eq. (3) requires the fragility curves, $F_{DS_{ij}}(\mathrm{EDP})$ and $F_{DS_{ij}}(\mathrm{GP})$, for the components that are dependent and independent of the geometric parameters, respectively. Such component fragility curves are characterized by a median value (=μ_{EDP}) and a dispersion factor (=$\beta_{\ln\mathrm{EDP}}$; lognormal standard deviation). Values of μ_{EDP} and $\beta_{\ln\mathrm{EDP}}$ for $F_{DS_{ij}}(\mathrm{EDP})$ are summarized in Table 1 with the information of repair time parameters $E[R_i|DS_{ij}]$ for each corresponding component and damage states. It is assumed that "Suspended ceiling" and "Automatic sprinklers" are hung from the top of each story and

"Elevator" is only affected by peak 1st-floor acceleration at 1st story. The component fragility parameters in Table 1 were based on [41,51] unless otherwise noted. The repair time parameters, $E[R_i|DM_{ij}]$, are the mean values retrieved from the fragility specification document (version 3.1.2) in Ref. [19]. Values of $\mu_{KL/r}$ and $\beta_{\ln KL/r}$ for $F_{DS_{ij}}(GP)$ are summarized in Table 2, which are based on [42]. The unit of the repair time used here is days/person. Note that in this study, only the dependence of global slenderness ratio (KL/r [42]) on the $F_{DS_{ij}}(GP)$ is considered. Furthermore, for buildings with SMFs, the dependence of geometric parameters on component fragility curves is not considered, thus $F_{DS_{ij}}(GP)$ in Eq. (3) is replaced with unity [52].

The repair of seismic isolation systems is not explicitly considered. Since the seismic isolation system considered in this study is located at the base, between the superstructure and the foundation, it is reasonable to assume that any inspection or repair action of the seismic isolation bearings does not contribute to the overall downtime. Experience from recent strong earthquake events showed that even if the seismic isolation bearings were damaged during strong motion excitation, they might be replaced without disrupting the building services [53].

This study considered four different types of seismic isolation systems for buildings with SCBF and SMF, as illustrated in Fig. 2. Those are: (*i*) triple friction pendulum [54] without moat wall (TFP-1); (*ii*) TFP with moat wall at the onset of hardening regime (TFP-1, with moat wall); (*iii*) TFP with larger displacement capacity without moat wall (TFP-3); and (*iv*) double concave friction pendulum bearing [55] without moat wall (DC-1). The size of isolation bearings of TFP-1 and DC-1 was determined based on the minimum requirement per ASCE/SEI 7–16 [31]. The details of designing seismic isolation bearings (TFP-1, TFP-3 and DC-1) can be found in Refs. [32–35]. Note that the TFP isolators do not have an interior restrainer ring. This type of isolators has been tested [56]. The bearing fails by exceeding the displacement limit when the rigid slider (the central part of TFP) slides off from the inner concave plates. The DC isolators do not have restrainer rings, which is nowadays a common practice in applications in Europe Ponzo et al. [57]. It should be noted that the current version of the European Standard EN15129 (CEN [58]; Section 8.3.1.2.3) prohibits the use of restrainer rings while ASCE/SEI 7–16 [31] does not have such requirement. The isolator displacement capacity, $D_{Capacity}$, for both TFP-1 and DC-1 isolators, was selected to meet the minimum requirements of standard ASCE/SEI 7–16 [31]. Thus, $D_{Capacity}$ needs to be equal to or larger than the maximum isolator displacement D_M calculated by the procedures of ASCE/SEI 7–16 (2017) for the MCE_R in the lower bound conditions of isolator properties [33,34]. For the TFP isolators, $D_{Capacity}$ was also selected to be the displacement at which initiation of stiffening occurs (for lower bound friction conditions). Both the TFP and DC isolators fail at the ultimate displacement, $D_{Ultimate}$, by exceeding the displacement limit when the rigid sliders (the central part of TFP and DC) slide off from the concave plates. $D_{Ultimate}$ is computed from $D_{Capacity}$ considering the size of rigid slider and hardening range (in case of TFP isolators), or considering just the size of the rigid slider (in case of DC isolators). Table 3 summarizes the properties of isolators, displacement capacities (i.e., "$D_{Capacity}$" and "$D_{Ultimate}$") and location of moat wall (placed at the "$D_{Capacity}$") for the considered isolators (see also Fig. 2).

4. Results and discussion on seismic downtime assessment

This section presents the results of the seismic downtime assessment based on the procedure presented in the previous section. The calculations of Equations (16) and (19) use seismic hazard data, which are obtained for the site (Latitude 37.783°, Longitude −122.392°) from the USGS website (https://earthquake.usgs.gov/hazards/interactive/[last accessed 25-Oct.2021]). For further information on the seismic hazard curves, the interested readers are referred to Refs. [32,33].

4.1. Mobilization time and probabilities of building safety tagging

As discussed in the previous section, the mobilization time when receiving different tagging (red, yellow or green) has an impact on the total computed downtime. This section examines the mobilization time and the probability of receiving different safety tags for seismically isolated and comparable non-isolated buildings based on the virtual inspector method proposed by Refs. [12,13]. As described in the introduction in this paper, the virtual inspector method determines the structural conditions using a red, yellow, or green placard based on the damage states of structural elements in the buildings, which are then translated into mobilization time using Eqs. 6–13 (see also Figs. 5 and 6). Fig. 7 presents the probability of receiving different colors of safety tags for selected structural systems. The probabilities shown in Fig. 7 are computed from Eqs. 6–13. Fig. 7 a, b presents the results for non-isolated buildings, with braced frame (a) and moment frame (b). It is seen that when using moment frames, the probability of receiving a yellow tag is high at all return periods. Fig. 7 c, d presents the results of seismically isolated buildings, with braced frame (c) and moment frame (d), designed with the smallest acceptable isolation bearings per ASCE/SEI 7–16 (2017) (TFP-1). In these cases, the probability of receiving a green tag dominates up to the return period of about 300 years. Fig. 7 e, f presents the results of seismically isolated buildings, with braced frame (e) and moment frame (f), with double concave (DC) bearings without any displacement restrainer. Fig. 7 e, f suggests that the buildings with DC isolators jump from a state of 100% probability of green tag to nearly 100% probability of red tag while slowly increasing return period. This is the consequence of reaching the ultimate displacement of the bearings (=$D_{Ultimate}$ in Fig. 2). The physical damage state when the probability of receiving red tag for DC isolators is due to the failure of isolators and thus the collapse of whole building. In reality, the physical damage state at the failure of DC isolators depends on how the seismic isolation systems are constructed. There may be some isolation systems where the superstructure overturns when the $D_{Ultimate}$ is exceeded, while there may be other isolation systems where the collapse of superstructure is

Table 3
Summary of seismic isolation system properties (for both SCBF and SMF buildings; see Fig. 2 for notations; friction properties are lower bound; properties in the table are used for both interior and exterior isolators).

	Radius of curvature		Friction coefficient		$D_{Capacity}$ (mm)	$D_{Ultimate}$ (mm)	Distance from the building to the moat wall (mm)
	Outer concave, $R_1 = R_4$ or R	Inner concave, $R_2 = R_3$	Outer concave, $\mu_1 = \mu_4$ or μ	Inner concave, $\mu_2 = \mu_3$			
TFP-1	2235	305	0.015	0.042	518	683	No wall
TFP-1 (with moat wall)	2235	305	0.015	0.042	518	683	+/− $D_{Capacity}$
TFP-3	2235	305	0.015	0.042	808	973	No wall
DC-1	2235	n/a	0.039	n/a	518	526	No wall

Height of outer concaves: $h_1+h_4 = 229$ mm for TFP-1 and TFP-3 ($h_1 = h_4$) and $2h = 229$ mm for DC-1. Height of inner concaves: $h_2 = h_3 = 152$ mm for TFP-1 and TFP-3 ($h_2 = h_3$). Heights are used to compute effective radius of curvatures ($R_{eff1} = R_1$-h_1; $R_{eff2} = R_2$-h_2; $R_{eff3} = R_3$-h_3; $R_{eff4} = R_4$-h_4; for TFP-1 and TFP-3, and $R_{eff} = R$-h for DC-1 — see Fig. 2).

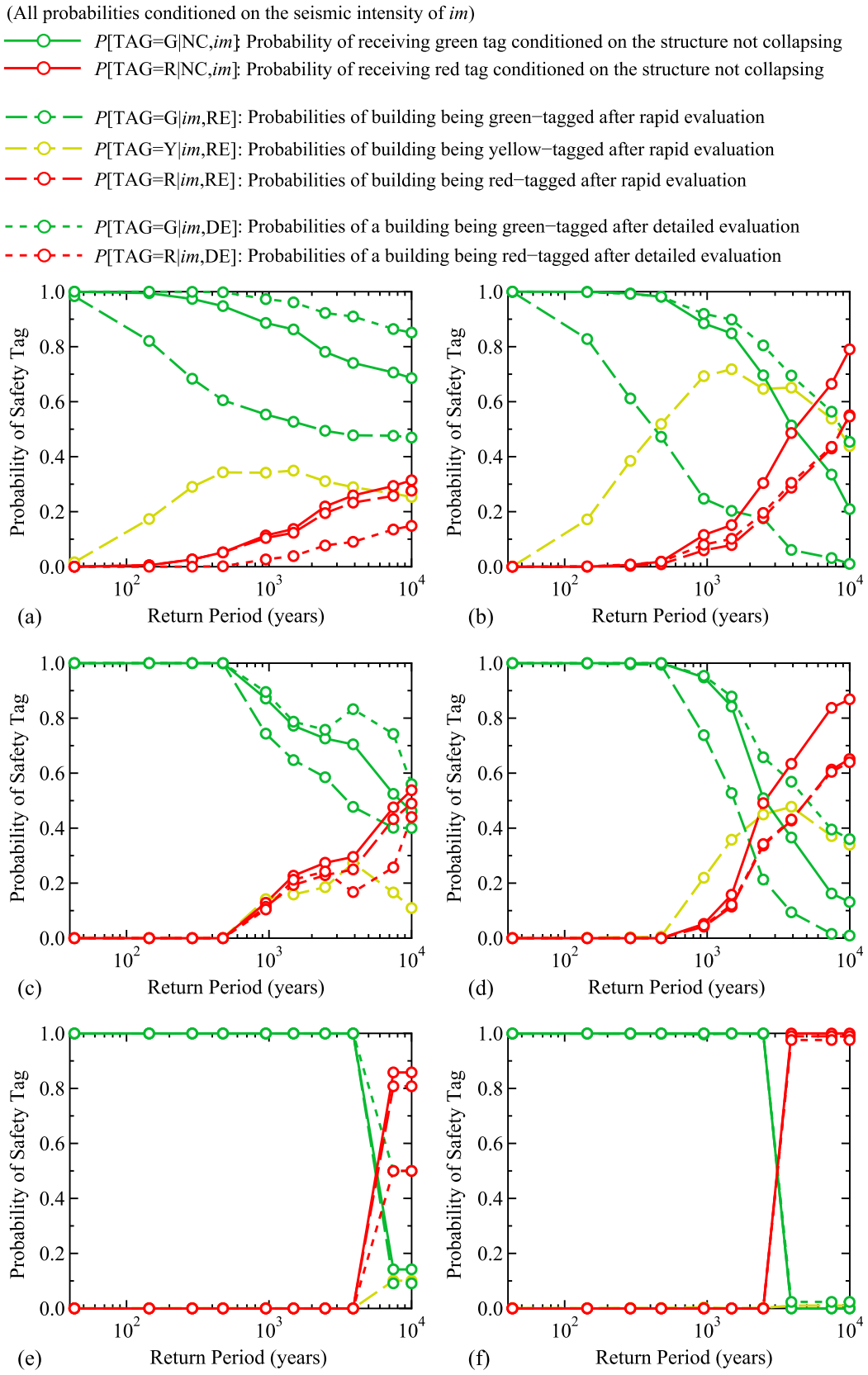

Fig. 7. Probabilities of receiving different safety tags for selected structural systems as a function of the seismic return period: (a) Non-isolated SCBF; (b) Non-isolated SMF; (c) Isolated SCBF designed with $R_I = 2$, with TFP-1 and with moat wall; (d) Isolated SMF designed with $R_I = 2$, with TFP-1 and with moat wall; (e) Isolated SCBF designed with $R_I = 2$, with DC-1 and without moat wall; (f) Isolated SMF designed with $R_I = 2$, with DC-1 and without moat wall.

Table 4
Mean mobilization times (times differ depending on which safety tags are assigned), $E[R_{T0}|NC, im]$

Return period (year)	43	144	289	475	949	1485	2475	3899	7462	10000
Structure	Mean mobilization times, $E[R_{T0}\|NC, im]$ (days)									
Non-isolated SCBF	10.0[a]	10.9	14.5	18.9	29.3	33.3	47.2	54.1	59.9	63.4
Isolated SCBF ($R_I = 1$) TFP-1	10.0[a]	10.0	10.0	10.0	10.1	11.5	19.9	19.2	36.3	52.0
Isolated SCBF ($R_I = 2$) TFP-1	10.0[a]	10.0	10.0	10.0	14.7	39.9	44.0	61.9	92.1	155.9
Isolated SCBF ($R_I = 2$) TFP-1 (with moat wall)	10.0[a]	10.0	10.0	10.0	31.9	48.6	56.6	60.2	90.8	101.4
Isolated SCBF ($R_I = 2$) TFP-3	10.0[a]	10.0	10.0	10.0	10.8	12.4	36.2	34.8	40.6	61.4
Isolated SCBF ($R_I = 2$) DC-1	10.0[a]	10.0	10.0	10.0	10.0	10.0	10.0	10.0	155.9	155.9
Non-isolated SMF	10.0[a]	10.1	11.1	13.1	29.6	35.8	61.7	92.7	123.0	144.4
Isolated SMF ($R_I = 1$) TFP-1	10.0[a]	10.0	10.0	10.0	11.8	13.9	59.0	56.4	80.8	124.0
Isolated SMF ($R_I = 2$) TFP-1	10.0[a]	10.0	10.0	10.0	14.7	33.9	87.8	99.4	138.9	140.1
Isolated SMF ($R_I = 2$) TFP-1 (with moat wall)	10.0[a]	10.0	10.0	10.0	18.8	36.8	93.5	117.8	152.4	157.6
Isolated SMF ($R_I = 2$) TFP-3	10.0[a]	10.0	10.0	10.0	12.7	28.7	72.4	90.5	106.2	124.7
Isolated SMF ($R_I = 2$) DC-1	10.0[a]	10.0	10.0	10.0	10.0	10.0	10.0	180.0	180.0	180.0

[a] The minimum of 10-days is due to the assumption of $E[R_{T0}|\text{TAG} = G] = 10$ (days) based on [12].

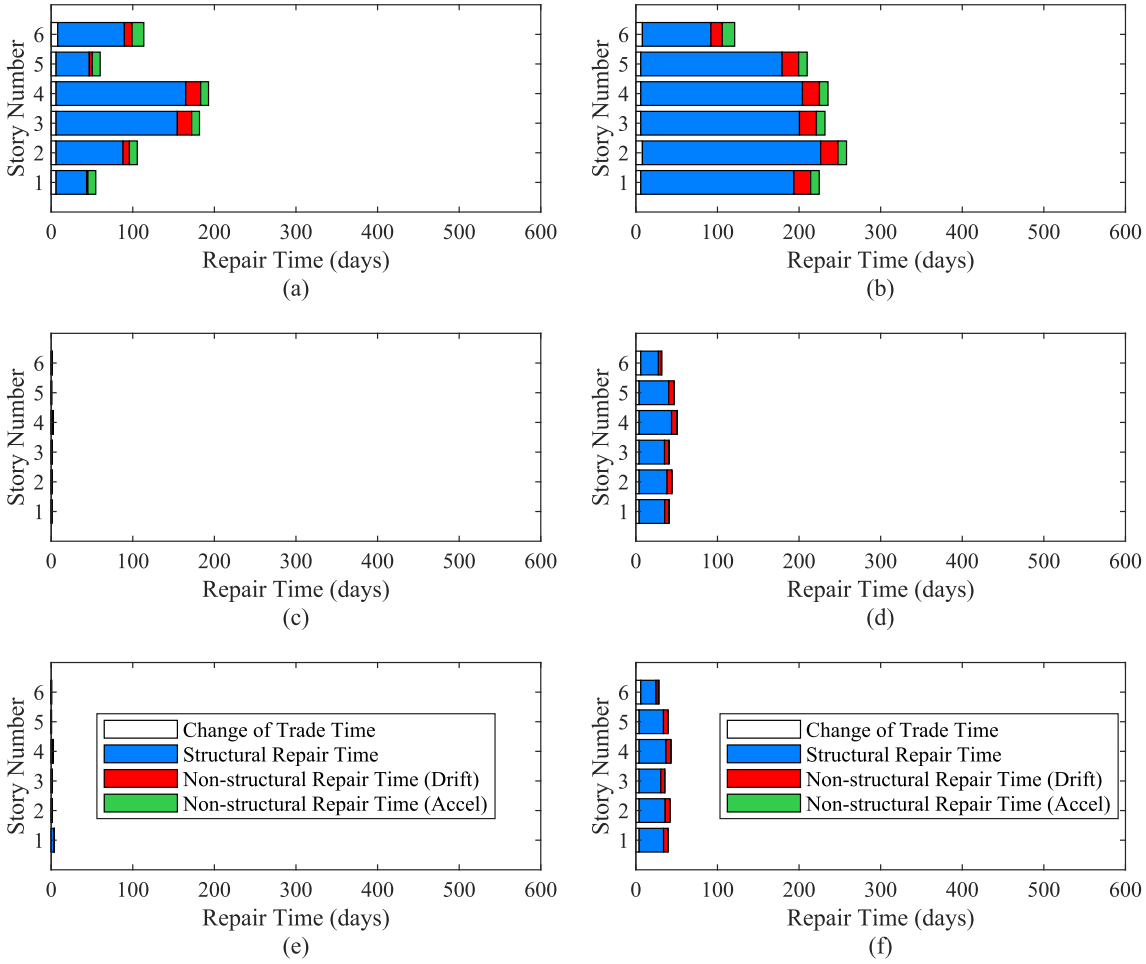

Fig. 8. Disaggregation of repair time (fast-track repair scheme) for selected structural systems under the earthquake scenario with a return period of 475 years: (a) Non-isolated SCBF; (b) Non-isolated SMF; (c) Isolated SCBF designed with $R_I = 2$, with TFP and with moat wall; (d) Isolated SMF designed with $R_I = 2$, with TFP and with moat wall; (e) Isolated SCBF designed with $R_I = 2$, with DC and without moat wall; (f) Isolated SMF designed with $R_I = 2$, with DC and without moat wall.

prevented by using vertical fail-safe systems that have been used in the past [59,60]. The computed mean mobilization times (i.e., tagging times), $E[R_{T0}|NC, im]$ in Eq. (6) are summarized in Table 4. Note that the minimum values of $E[R_{T0}|NC, im]$ for all buildings are 10-days. This is because of the assumption that even receiving a green tag will take 10-days (i.e., $E[R_{T0}|\text{TAG} = G] = 10$ (days) based on [12]; see Eq. (6)). It is noted that the computation of downtime, $E[R_{T+T0}|\text{NC}, im]$, in Eq. (5) by calculating the sum of repair time and the mobilization time may be conservative as it turned out that the seismically isolated buildings in the recent strong earthquake event did not experience any downtime [53]. Also note that if other elements of mobilization times are included (ex. consultation with professional engineers and/or contractor bidding process), the mobilization times in Table 4 might have become larger.

4.2. Downtime disaggregation results

As discussed in the previous sections, downtime is the summation of the rational component (i.e., repair time in this study) and the irrational

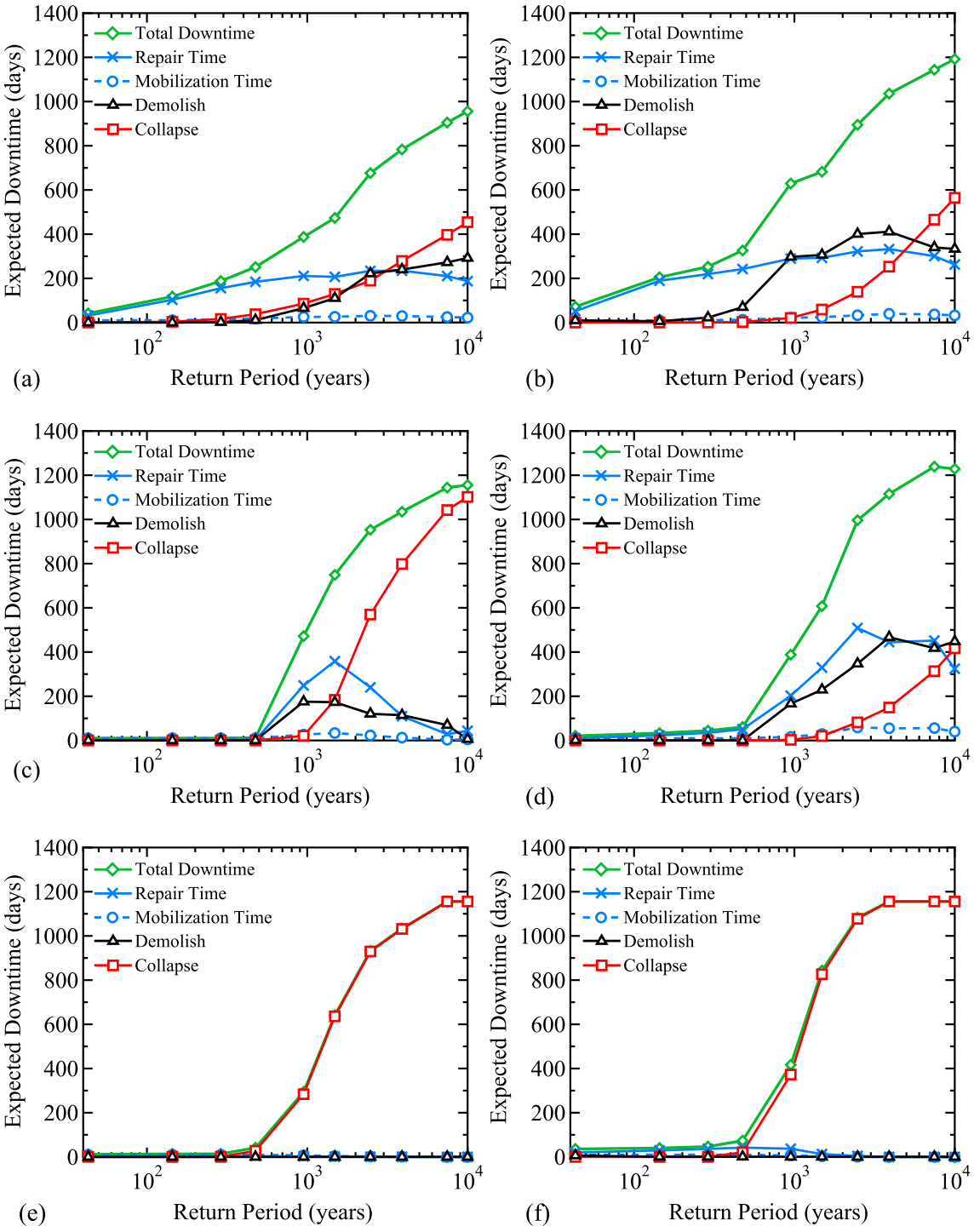

Fig. 9. Downtime vulnerability curves for selected structural systems: (a) Non-isolated SCBF; (b) Non-isolated SMF; (c) Isolated SCBF designed with $R_I = 2$, with TFP-1 and with moat wall; (d) Isolated SMF designed with $R_I = 2$, with TFP-1 and with moat wall; (e) Isolated SCBF designed with $R_I = 2$, with DC-1 and without moat wall; (f) Isolated SMF designed with $R_I = 2$, with DC-1 and without moat wall.

component (i.e., mobilization or safety tagging time in this study). In this section, the repair time is disaggregated into the repair times of change-of-trade, structural components, and drift- and acceleration-sensitive nonstructural components, for each operational unit and for a specific return period of 475 years. According to Molina Hutt et al. [15], the selected intensity level (= return period of 475 years) is representative of the expected earthquake used by the San Francisco Planning and Urban Research Association to define resilience. This expected earthquake corresponds to a magnitude 7.2 earthquake scenario, which is an event that can be expected conservatively, but reasonably within the lifetime of a structure. Fig. 8 presents the results of computations of repair times when the repairs were conducted in a fast-track repair scheme. It is seen that the seismically isolated buildings have reduced repair times in comparison to the non-isolated buildings. In all the structural systems presented in Fig. 8, the repair time for structural components dominates in comparison with other sources of repair times. The reason for this result is that the repair time for corrugated slabs was estimated using the fragility parameters that were conservative (fragility data based on the [12]. Recent technology advancement might have improved the seismic performance of the corrugated slabs (structural component), consequently reducing the corresponding repair time. Also, the reason behind the small contribution to the repair times from non-structural components may be that some of the components were assumed to be braced (i.e, automatic sprinklers) or supported (i.e., suspended ceilings). The fragility parameters of these braced or supported non-structural components are less sensitive to small floor accelerations or small story drifts, thus the small values might be calculated for the corresponding repair times. The computed values for isolated and non-isolated buildings are generally consistent with the results reported in Ref. [15].

4.3. Downtime vulnerability functions

Fig. 9 presents the downtime vulnerability curves of selected buildings for fast-track repair scheme. Downtime vulnerability curves are the probabilistic distribution of downtime at each earthquake intensity. The downtime vulnerability curves are provided in Fig. 9 for the rational component of downtime (i.e., repair time), the irrational component of downtime (i.e., mobilization time), and the times due to demolition and collapse. These are computed as follows (also see Equations (5) and (14)):

$$E[R_{\mathrm{T}}|\mathrm{NC}, im] \bullet (1 - P[D|IM, NC]) \bullet (1 - P[C|IM]) \quad \text{(Repair time)} \tag{20}$$

$$E[R_{\mathrm{T0}}|\mathrm{NC}, im] \bullet (1 - P[D|IM, NC]) \bullet (1 - P[C|IM]) \quad \text{(Mobilization time)} \tag{21}$$

$$[D_{\mathrm{T}}|\mathrm{NC}] \bullet P[D|IM, NC] \bullet (1 - P[C|IM]) \quad \text{(Demolish)} \tag{22}$$

$$E[C_{\mathrm{T}}|\mathrm{C}] \bullet P[C|IM] \quad \text{(Collapse)} \tag{23}$$

Fig. 9 shows that the repair time contributes significantly to the total downtime of non-isolated buildings, whereas the time when collapse occurs contributes significantly to the total downtime of isolated buildings. It is seen that when DC bearings are used for seismic isolation systems, the total downtime vulnerability curves are nearly identical to the collapse vulnerability curves. The contribution of demolition time (i.e., demolition due to the large permanent deformation) to the total downtime is large for buildings with SMFs, especially when the buildings are non-isolated buildings. Note that the repair time is large (about 70 days for non-isolated buildings) even at the smallest return period. This is because of the fragility properties for braced automatic sprinklers (acceleration-sensitive non-structural component, see Table 1) that have a high value of uncertainty ($\beta_{\mathrm{lnEDP}} = 1.4$). The parameters of the fragility curve for braced automatic sprinklers were based on the data from a document that was published many years ago (B.5.1 in Porter and Kiremidjian [43]) and the seismic performance of automatic sprinklers might have been improved since then. Recently, Ref. [61] showed that the non-structural repairs and impeding factor delays of non-isolated 50-story steel moment resisting frame buildings were the greatest downtime contributors. However, Fig. 9 points to a somewhat small contribution of "mobilization time" (or impeding factors) to the total downtime. Nevertheless, Ref. [61] studied a high-rise building (50-story in contrast with 6-story buildings in this paper) and considered other elements of mobilization times, such as financing, permitting and review/re-design based on REDi™ [5,9]. These two factors (structural height and the definition of mobilization time) may justify the differences between the two studies in the estimated contributions of mobilization times in the total downtime.

4.4. Expected annual downtime

Table 5 presents the expected annual downtime (*EADT*) evaluated from Equation (16) for both fast- and slow-track repair strategies. It is seen from the table that the *EADTs* of all seismically isolated buildings are less than the *EADTs* of the corresponding non-isolated buildings regardless of the repair strategy. It is also found that when the seismically isolated buildings are designed with SCBFs, $R_{\mathrm{I}} = 2$ and TFP-3, the computed *EADT* becomes minimum among all the considered cases of buildings. This implies that the use of stiff superstructure and the introduction of reserve displacement capacity through TFP-3 are beneficial for the reduction of downtime. Also, when *EADTs* are compared between the DC and TFP isolators with the minimum required displacement capacities per ASCE/SEI 7–16 [31], the TFP (i.e., TFP-1) resulted in the lower *EADTs* than DC (i.e., DC-1) for both SCBF and SMF.

4.5. Expected annual downtime losses

Table 6 presents the expected annual downtime losses (*EADTL*) evaluated from Equation (19) for both fast- and slow-track repair strategies. It is seen from the table that the computed values of *EADTL* of all seismically isolated buildings are less than the values of *EADTL* of the corresponding non-isolated buildings regardless of the repair strategy. It is also found that when the seismically isolated buildings are designed with SCBFs, $R_{\mathrm{I}} = 2$ and TFP-3, the computed *EADTL* becomes minimum among all the considered cases of buildings.

Previous study by Kitayama and Constantinou [35] showed that using moat wall for the seismically isolated buildings with isolators designed by the minimum requirement of ASCE/SEI 7–16 [31] led to the improvement of collapse performance when the isolation systems between DC-1 isolators (without moat wall) and TFP-1 isolators (with moat wall – which is equivalent to the DC-1 with moat wall) were compared but led to the no-effect or slightly deteriorating effect (depending on the superstructure system used, i.e., SCBF or SMF) when the isolation systems between TFP-1 isolators (without moat wall) and

Table 5
Expected annual downtime (*EADT*).

Structure types	Size and type of isolators*[1]	Fast-track repair strategy (days)	Slow-track repair strategy (days)
Non-isolated SCBF	NA	1.6	5.4
Isolated SCBF ($R_I = 1$)	TFP-1	0.6	0.7
Isolated SCBF ($R_I = 2$)	TFP-1	0.7	0.8
Isolated SCBF ($R_I = 2$)	TFP-1 (with moat wall)	0.8	1.0
Isolated SCBF ($R_I = 2$)	TFP-3	0.5	0.6
Isolated SCBF ($R_I = 2$)	DC-1	0.8	0.8
Non-isolated SMF	NA	2.4	10.7
Isolated SMF ($R_I = 1$)	TFP-1	0.8	3.5
Isolated SMF ($R_I = 2$)	TFP-1	0.9	4.4
Isolated SMF ($R_I = 2$)	TFP-1 (with moat wall)	1.0	4.7
Isolated SMF ($R_I = 2$)	TFP-3	0.9	4.3
Isolated SMF ($R_I = 2$)	DC-1	1.3	4.7

*[1]: For detail of notations, see Fig. 1.

Table 6
Expected annual downtime losses (*EADTL*).

Structure types	Size and type of isolators*[1]	Fast-track repair strategy (USD)	Slow-track repair strategy (USD)
Non-isolated SCBF	NA	3,497	6,734
Isolated SCBF ($R_I = 1$)	TFP-1	2,646	2,742
Isolated SCBF ($R_I = 2$)	TFP-1	2,866	3,016
Isolated SCBF ($R_I = 2$)	TFP-1 (with moat wall)	3,134	3,330
Isolated SCBF ($R_I = 2$)	TFP-3	2,220	2,313
Isolated SCBF ($R_I = 2$)	DC-1	3,672	3,710
Non-isolated SMF	NA	5,212	12,156
Isolated SMF ($R_I = 1$)	TFP-1	2,830	5,055
Isolated SMF ($R_I = 2$)	TFP-1	2,832	5,721
Isolated SMF ($R_I = 2$)	TFP-1 (with moat wall)	2,834	5,957
Isolated SMF ($R_I = 2$)	TFP-3	2,528	5,414
Isolated SMF ($R_I = 2$)	DC-1	5,097	7,955

*[1]: For detail of notations, see Fig. 1.

TFP-1 isolators (with moat wall) were compared. These trends were also observed for the results of downtime evaluation (Tables 5 and 6) because the evaluation of downtime (i.e., inspection and repair times) are primarily dependent on the collapse probability of the seismically isolated buildings, as shown in Fig. 9.

5. Conclusion

This paper demonstrated the downtime assessment of seismically isolated and non-isolated steel framed buildings. The study considered 6-story office buildings located in California that were designed based on the seismic design standard, ASCE/SEI 7–16 [31]. The data from the results of nonlinear response history analyses in Refs. [32,33] were used to evaluate the downtime of seismically isolated buildings and comparable non-isolated buildings. Different strengths of isolated buildings and different types of seismic isolation systems including two different sliding seismic isolation systems with and without moat walls were considered. The main findings are summarized as follows:

1. The mean mobilization times of seismically isolated buildings under frequent to moderately rare earthquake events (characterized by return periods of up to 949 years) were less than the mean mobilization times of comparable non-isolated buildings.
2. The probabilities of receiving green tags for seismically isolated buildings were higher under frequent earthquake motions than those for non-isolated buildings. The non-isolated buildings may receive a yellow tag even under frequently occurring earthquake event with low return period.
3. The computed total repair times under the earthquake with a return period of 475 years were about 200 days for non-isolated buildings. For seismically isolated buildings, the total repair times were about a few days (with SCBFs) and 50 days (with SMFs).
4. Generally, seismically isolated buildings with moment frames required longer downtimes than the seismically isolated buildings with braced frames.
5. The estimated expected annual downtimes of seismically isolated buildings were less than the downtimes of comparable non-isolated buildings regardless of the repair scheme (fast or slow) and regardless of the seismic isolation system considered.

Other downtime components, such as engineering mobilization, contractor mobilization or financing, were not considered in this work due to insufficient information available for their estimation. Nevertheless, consideration of such components is expected to increase the downtime estimates of the non-isolated buildings and therefore reinforce the findings presented herein, i.e., that seismically isolated systems are more viable economical and resilient than non-isolated ones.

Author statement

All persons who meet authorship criteria are listed as authors, and all authors certify that they have participated sufficiently in the work to take public responsibility for the content, including participation in the concept, design, analysis, writing, or revision of the manuscript. Furthermore, each author certifies that this material or similar material has not been and will not be submitted to or published in any other publication before its appearance in the **Soil Dynamics and Earthquake Engineering**. The following indicates the specific contributions made by each author:

Shoma Kitayama: Conceptualization, Methodology, Software development, Original draft preparation. Enrique Abel Morales Moncayo: Reviewing, Editing and Draft preparation. Anastasia Athanasiou: Reviewing, Editing, and Draft preparation.

Declaration of competing interest

The authors declare that they have no known competing financial interests or personal relationships that could have appeared to influence the work reported in this paper.

Data availability

Data will be made available on request.

Acknowledgement

Most of the works in this paper were conducted when the first and the second authors were employed by the University at Buffalo, State University of New York, New York, USA. The writers acknowledge the support from SUNY Distinguished Professor Michael C. Constantinou in the Department of Civil, Structural and Environmental Engineering at the University at Buffalo, State University of New York. Site visits to observe the aftermath of the 2016 Ecuador earthquake helped shape the work in this paper. The authors acknowledge the travel support provided to the first author by the Armed Forces University (ESPE).

References

[1] Zayas V, Mahin S, Constantinou M. Seismic isolation standard for continued functionality. In: *Proc., 17th U.S.-Japan-New Zealand Workshop on the Improvement of structural Engineering and resilience*. Rydges lakeland resort. Queenstown. New Zealand: Applied Technology Council (ATC); 2018.
[2] Ceferino L, Mitrani-Reiser J, Kiremidjian A, Deierlein G, Bambarén C. Effective plans for hospital system response to earthquake emergencies. Nat Commun 2020; 11(4325). https://doi.org/10.1038/s41467-020-18072-w.
[3] Brookshire DS, Chang S-E, Cochrane H, Olson RA, Rose A, Steenson J. Direct and indirect economic losses from earthquake damage. Earthq Spectra 1997;13(4): 683–701. https://doi.org/10.1193/1.1585975.
[4] Kitayama S, Cilsalar H. Seismic loss assessment of seismically isolated buildings designed by the procedures of ASCE/SEI 7-16. Bull Earthq Eng 2022;20:1143–68. https://doi.org/10.1007/s10518-021-01274-y.
[5] Almufti I, Willford M. The REDi^{TM} rating system: a framework to implement resilience-based earthquake design for new buildings. In: *Proc., tenth U.S. National Conference on earthquake engineering Frontiers of earthquake engineering*. Anchorage, Alaska, USA: National Conference on Earthquake Engineering; 2014.
[6] Bonowitz D. Resilience criteria for seismic evaluation of existing buildings: a proposal to supplement ASCE 31 for intermediate performance objectives. In: *Proc., Improving the seismic Performance of existing Buildings and other structures*. San Francisco, California, USA: Applied Technology Council (ATC) and Structural Engineering Institute (SEI); 2009. https://doi.org/10.1061/9780784410844.
[7] SEAONC (Structural Engineers Association of Northern California). SEAONC rating system for the expected earthquake performance of buildings." 2011 SEAOC Convention Proceedings, Las Vegas. NV, USA: Structural Engineers Association of Northern California; 2011. https://www.seao.org/sites/default/files/files/content/SEAONC%20Rating%20System.pdf.
[8] USRC (U.S. Resiliency Council). Implementation manual. USRC building rating system for earthquake hazards. https://www.usrc.org/wp-content/uploads/USRC-Implementation-Manual-Final.pdf. [Accessed 19 March 2022].
[9] Almufti I, Willford M. *Resilience-based earthquake design initiative (REDi^{TM}) rating system*. San Francisco, CA, USA: Arup; 2013. Arup, https://www.arup.com/perspectives/publications/research/section/redi-rating-system.

[10] Comerio MC. Estimating downtime in loss modeling. Earthq Spectra 2006;22(2):349–65. https://doi.org/10.1193/1.2191017.

[11] Mayes R, Tam K, Weaver B, Wetzel N, Parker W, Brown A, Pietra D. Performance based design of buildings to assess damage and downtime and implement a rating system. Bull N Z Soc Earthq Eng 2013;46(1):40–55. http://www.nzsee.org.nz/db/Bulletin/Archive/46(1)0040.pdf.

[12] Mitrani-Reiser J. An ounce of prevention: probabilistic loss estimation for performance-based earthquake engineering. Ph.D. Dissertation. Pasadena, CA, USA: California Institute of Technology; 2007.

[13] Mitrani-Reiser J, Wu S, Beck JL. Virtual Inspector and its application to immediate pre-event and post-event earthquake loss and safety assessment of buildings. Nat Hazards 2016;81:1861–78. https://doi.org/10.1007/s11069-016-2159-6.

[14] ATC (Applied Technology Council). ATC-20, Procedures for post-earthquake safety evaluation of buildings. Redwood City, CA, USA: ATC; 1989.

[15] Molina Hutt C, Almufti I, Willford M, Deierlein D. Seismic loss and downtime assessment of existing tall steel-framed buildings and strategies for increased resilience. J Struct Eng 2016;142(8):C4015005. https://doi.org/10.1061/(ASCE)ST.1943-541X.0001314.

[16] Kammouh O, Cimellaro GP, Mahin SA. Downtime estimation and analysis of lifelines after an earthquake. Eng Struct 2018;173(15):393–403. https://doi.org/10.1016/j.engstruct.2018.06.093.

[17] Porter KA, Kiremidjian AS, LeGrue JS. Assembly-based vulnerability of buildings and its use in performance evaluation. Earthq Spectra 2001;17(2):291–312. https://doi.org/10.1193/1.1586176.

[18] Beck JL, Kiremidjian A, Wilkie S, Mason A, Salmo T, Goltz J, Olson R, Workman J, Irfanoglu A, Porter KA. *Decision support tools for earthquake recovery of business*. Final Report for CUREe-Kajima Phase III Project. Richmond, CA, USA: Consortium of Universities for Research in Earthquake Engineering; 1999.

[19] FEMA (Federal Emergency Management Agency). *Seismic performance assessment of buildings*. FEMA P-58, Fragility Specification. third ed. Washington, DC, USA: Applied Technology Council for the Federal Emergency Management Agency; 2018.

[20] Mieler MW, Mitrani-Reiser J. Review of the state of the art in assessing earthquake-induced loss of functionality in buildings. J Struct Eng 2018;144(3):04017218. https://doi.org/10.1061/(ASCE)ST.1943-541X.0001959.

[21] Molina Hutt C, Hulsey AM, Kakoty P, Deierlein GG, Monfared AE, Yen W-Y, Hooper JD. Toward functional recovery performance in the seismic design of modern tall buildings. Earthq Spectra 2022;38(1):283–309. https://doi.org/10.1177/87552930211033620.

[22] FEMA (Federal Emergency Management Agency). *Seismic performance assessment of buildings*. FEMA P-58. Washington, DC, USA: Applied Technology Council for the Federal Emergency Management Agency; 2012.

[23] Terzic V, Merrifield SK, Mahin SA. Lifecycle cost comparisons for different structural systems designed for the same location. In: *Proc., 15th world Conference on earthquake engineering*, lisbon, Portugal; 2012.

[24] ASCE (American Society of Civil Engineers). Minimum design loads for buildings and other structures. Reston, VA: ASCE; 2005. ASCE/SEI 7-05.

[25] Moretti, S., Trozzo, A., Terzic, V., Cimellaro, G. P., and Mahin, S. 2014. "Utilizing base-isolation systems to increase earthquake resiliency of healthcare and school buildings." In Proc., 4th International Conference on Building Resilience, edited by Procedia Economics and Finance, 18, 969-976. Salford Quays, UK. https://doi.org/10.1016/S2212-5671(14)01024-7.

[26] Cimellaro GP, Terzic V, Mahin S. Quantification of resilience improvements for critical facilities through advanced technologies. In: *Proc., 12th international Conference on Applications of Statistics and Probability in Civil engineering, ICASP12*, vancouver, Canada: Civil engineering risk and reliability association (CERRA); 2015.

[27] ASCE (American Society of Civil Engineers). Minimum design loads for buildings and other structures. Reston, VA: ASCE; 2010. ASCE/SEI 7-10.

[28] Cutfield M, Ryan K, Ma Q. Comparative life cycle analysis of conventional and base-isolated buildings. Earthq Spectra 2016;32(1):323–43. https://doi.org/10.1193/032414EQS040M.

[29] ICBO (International Conference of Building Officials). Uniform building code: structural engineering design provisions, vol. 2. Whittier, CA, USA: International Conference of Building Officials (International Code Council; 1997.

[30] Dong Y, Frangopol DM. Performance-based seismic assessment of conventional and base-isolated steel buildings including environmental impact and resilience. Earthq Eng Struct Dynam 2016;45(4):739–56. https://doi.org/10.1002/eqe.2682.

[31] ASCE (American Society of Civil Engineers). Minimum design loads and associated criteria for buildings and other structures. Reston, VA: ASCE; 2017. ASCE/SEI 7-16.

[32] Kitayama S, Constantinou MC. Probabilistic seismic performance assessment of seismically isolated buildings designed by the procedures of ASCE/SEI 7 and other enhanced criteria. Eng Struct 2019;179:566–82. https://doi.org/10.1016/j.engstruct.2018.11.014.

[33] Kitayama S, Constantinou MC. Seismic performance assessment of seismically isolated buildings designed by the procedures of ASCE/SEI 7. MCEER-18-0004. Buffalo, NY, USA: Multidisciplinary Center for Earthquake Engineering Research; 2018.

[34] Kitayama S, Constantinou MC. Collapse performance of seismically isolated buildings designed by the procedures of ASCE/SEI 7. Eng Struct 2018;164:243–58. https://doi.org/10.1016/j.engstruct.2018.03.008.

[35] Kitayama S, Constantinou MC. Effect of displacement restraint on the collapse performance of seismically isolated buildings. Bull Earthq Eng 2019;17:2767–86. https://doi.org/10.1007/s10518-019-00554-y.

[36] Ramirez CM, Miranda E. Significance of residual drifts in building earthquake loss estimation. Earthq Eng Struct Dynam 2012;41(11):1477–93. https://doi.org/10.1002/eqe.2217.

[37] Kitayama S, Moncayo EAM, Athanasiou A. MATLAB code for downtime assessment of seismically isolated buildings. 2022. https://github.com/shkma/Downtime. [Accessed 10 April 2022].

[38] NIST (National Institute of Standards and Technology). Selecting and scaling earthquake ground motions for performing response-history analysis. NIST GCR 11-917-15. Technical Report. Gaithersburg, Maryland, USA: NEHRP consultants joint venture for the National Institute of Standards and Technology; 2011.

[39] Lin T, Haselton CB, Baker JW. Conditional spectrum-based ground motion selection. Part I: hazard consistency for risk-based assessments. Earthq Eng Struct Dynam 2013;42(12):1847–65. https://doi.org/10.1002/eqe.2301.

[40] Baker JW. Conditional mean spectrum: Tool for ground-motion selection. J Struct Eng 2011;137(3):332–44. https://doi.org/10.1061/(ASCE)ST.1943-541X.0000215.

[41] Hwang SH, Lignos DG. Effect of modeling assumptions on the earthquake-induced losses and collapse risk of steel-frame buildings with special concentrically braced frames. J Struct Eng 2017;143(9):04017116. https://doi.org/10.1061/(ASCE)ST.1943-541X.0001851.

[42] Lignos DG, Karamanci E. Drift-Based and dual-parameter fragility curves for concentrically braced frames in seismic regions. J Constr Steel Res 2013;90:209–20. https://doi.org/10.1016/j.jcsr.2013.07.034.

[43] Porter KA, Kiremidjian AS. Assembly-based vulnerability of buildings and its uses in seismic performance evaluation and risk management decision-making. Report No. 139. Stanford, CA, USA: The Blume Earthquake Engineering Center. Department of Civil and Environmental Engineering. Stanford University; 2001.

[44] ATC (Applied Technology Council). ATC-20, Procedures for post-earthquake building safety evaluation procedures. Redwood City, CA, USA: ATC; 1995.

[45] Anagnostopoulos S, Moretti M. Post-earthquake emergency assessment of building damage, safety and usability-Part 2: Organisation. Soil Dynam Earthq Eng 2008;28(3):233–44. https://doi.org/10.1016/j.soildyn.2006.05.008.

[46] Allali SA, Abed M, Mebarki A. Post-earthquake assessment of buildings damage using fuzzy logic. Eng Struct 2018;166(1):117–27. https://doi.org/10.1016/j.engstruct.2018.03.055.

[47] Mangalathu S, Sun H, Nweke CC, Yi Z, Burton HV. Classifying earthquake damage to buildings using machine learning. Earthq Spectra 2020;36(1):183–208. https://doi.org/10.1177/8755293019878137.

[48] Comerio MC, Blecher HE. Estimating downtime from data on residential buildings after the northridge and loma prieta earthquakes. Earthq Spectra 2010;26(4):951–65. https://doi.org/10.1193/1.3477993.

[49] Okada S, Takai N. Classifications of structural types and damage patterns of buildings for earthquake field investigation. In: *Proc., 12th world Conference on earthquake engineering*. Auckland, New Zeland: New Zealand Society for Earthquake Engineering; 2000.

[50] Adam JM, Parisi F, Sagaseta J, Lu X. Research and practice on progressive collapse and robustness of building structures in the 21st century. Eng Struct 2018;173(15):122–49. https://doi.org/10.1016/j.engstruct.2018.06.082.

[51] Hwang SH, Lignos DG. Earthquake-induced loss assessment of steel frame buildings with special moment frames designed in highly seismic regions. Earthq Eng Struct Dynam 2017;46(13):2141–62. https://doi.org/10.1002/eqe.2898.

[52] Porter K, Kennedy R, Bachman R. Creating fragility functions for performance-based earthquake engineering. Earthq Spectra 2007;23(2):471–89. https://doi.org/10.1193/1.2720892.

[53] Kani N, Ogino N, Kitamura Y, Kitamura H. Effects of seismically-isolated buildings during the huge 2011 earthquake in Japan. In: *Proc., 15th world Conference on earthquake engineering*. Lisbon, Portugal: Sociedade Portuguesa de Engenharia Sísmica; 2012.

[54] Fenz DM, Constantinou MC. Spherical sliding isolation bearings with adaptive behavior: Theory. Earthq Eng Struct Dynam 2008;37(2):163–83. https://doi.org/10.1002/eqe.751.

[55] Fenz DM, Constantinou MC. Behaviour of the double concave friction pendulum bearing. Earthq Eng Struct Dynam 2006;35(11):1403–24. https://doi.org/10.1002/eqe.589.

[56] Lee D, Constantinou MC. Combined horizontal-vertical seismic isolation system for high-voltage power transformers: development, testing and validation. Bull Earthq Eng 2018;16:4273–96. https://doi.org/10.1007/s10518-018-0311-2.

[57] Ponzo FC, Cesare AD, Leccese G, Nigro D. Shake table testing on restoring capability of double concave friction pendulum seismic isolation systems. Earthquake. Eng. Struct Dyn. 2017;46(14):2337–53. https://doi.org/10.1002/eqe.2907.

[58] CEN European Standard EN15129: Anti-seismic devices. Brussels, Belgium: European Committee for Standardization; 2018.

[59] Kelly JM, Beucke KE. A friction damped base isolation system with fail-safe characteristics. Earthq Eng Struct Dynam 1983;11(1):33–56. https://doi.org/10.1002/eqe.4290110105.

[60] Tarics AG, Way D, Kelly JM. The implementation of base isolation for the foothill communities law and justice center." county of san bernardino, California. A report to the national science foundation and the county of san bernardino. 1984. Report no. NSF/CEE-84041.

[61] Molina Hutt C, Rossetto T, Deierlein D. Comparative risk-based seismic assessment of 1970s vs modern tall steel moment frames. J Constr Steel Res 2019;159(8):598–610. https://doi.org/10.1016/j.jcsr.2019.05.012.